Supplementary Information for:

Manganese doped-iron oxide nanoparticle secondary structures and their potential as agents for magnetic resonance imaging and hyper-thermia

Maria F. Casula, [♂,¶] Erika Conca, [♂,¶] Ioanna Bakaimi,[¥] Ayyappan Sathya,[♊] Maria Elena Materia,[♊] Alberto Casu, [≠] Andrea Falqui,[≠] Elisa Sogne, [≠] Teresa Pellegrino,[♊] and Antonios G. Kanaras[¥,*]

[¥] Institute for Life Sciences, Physics and Astronomy, Faculty of Physical Sciences and Engineering, University of Southampton, Southampton, SO17 1BJ, United Kingdom.

[♂]Department of Chemical and Geological Sciences and INSTM, University of Cagliari, 09042 Monserrato, Italy.

[♊]Istituto Italiano di Tecnologia, via Morego 30, 16145 Genoa, Italy.

[≠]Biological and Environmental Science and Engineering Division, KAUST, Jeddah, Saudi Arabia.

[¶]These authors contributed equally in this work.

Table of Contents

S1. Mn-doped iron oxide cluster distribution.

S2. Structural and elemental characterization of Mn-doped iron oxide clusters.

S3. ^{1}H Relaxivity values of Mn-doped iron oxide clusters: dependence from the magnetic field.

S4. SAR values of Mn-doped iron oxide clusters: dependence from magnetic field.

S5. SAR values of Mn-doped iron oxide cluster from temperature kinetic curves.

S6. SAR values and physicochemical characterization of undoped iron oxide clusters.

S1. Mn-doped iron oxide cluster distribution.

Size distribution of the CNCs samples were determined by analysing the TEM images with the free-ware ImageJ software (http://imagej.nih.gov/ij/). The mean cluster diameter and size distribution were obtained from a statistical analysis over about 300 particles by fitting with a log-normal distribution. The average distribution of the inorganic clusters is 51±15 nm.

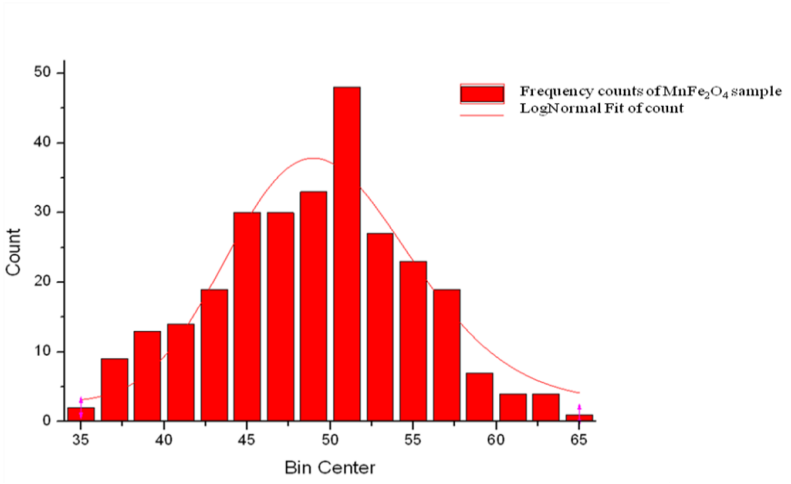

Figure S1. Mn-doped Cluster Size distribution plot as obtained by statistical analysis of TEM images.

The hydrodynamic diameter of the Mn-doped iron oxide clusters was determined by dynamic light spectroscopy. The hydrodynamic average size of the clusters was 54±19 nm. The hydrodynamic average size is slighter higher than the size of the clusters estimated by TEM due to the presence of the PAA polymer on the cluster surface.

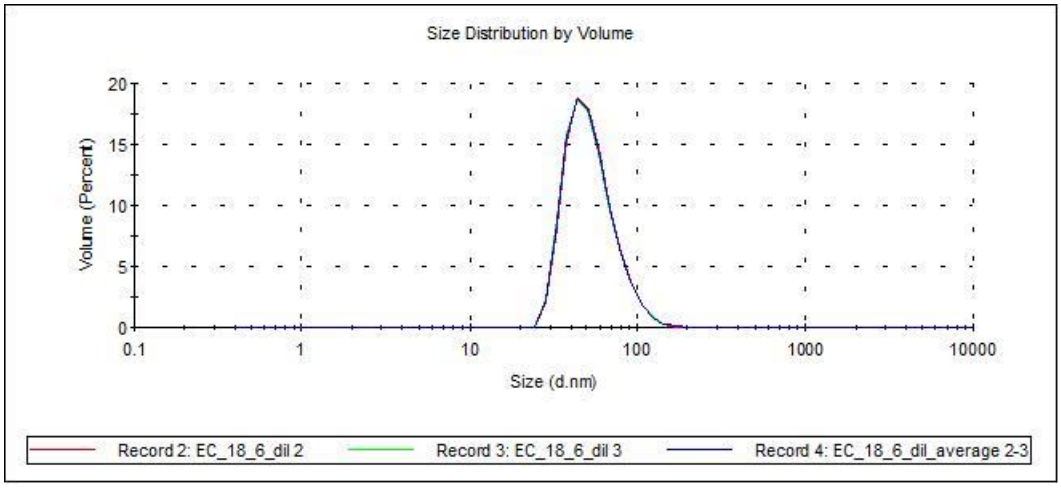

Figure S2. Dynamic light scattering size distribution of Mn-doped iron oxide clusters

S2. Structural and elemental characterization of Mn-doped iron oxide clusters.

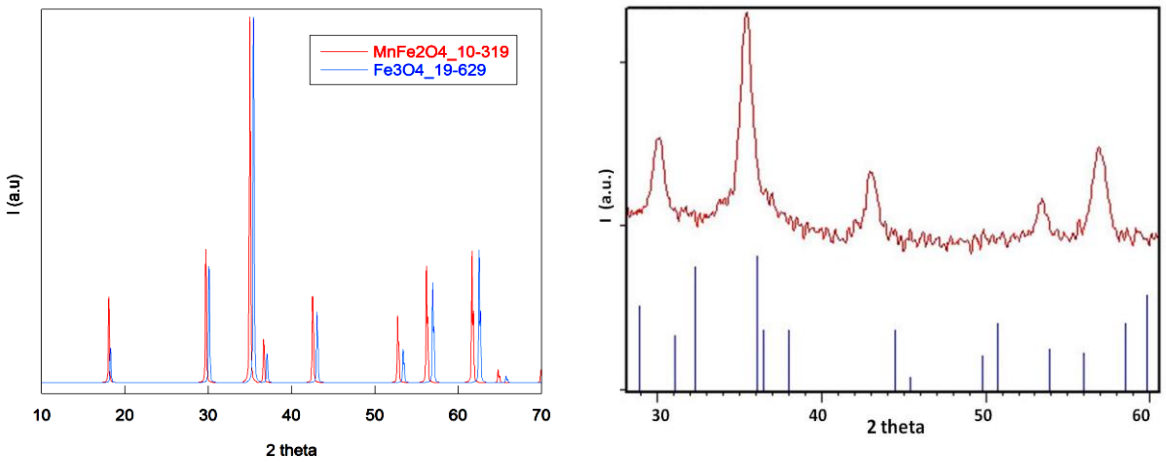

Figure S3. (A) Simulated X-ray diffraction pattern for $MnFe_2O_4$ (PDF card 10-319) and Fe_3O_4 (PDF card 19-629). (B) The experimental X-ray diffraction pattern for MnFe2O4: as demonstrated by comparison with the reference reflections of pure Mn3O4 (PDF card 24-734), the occurrence of man-ganese oxide phases can be ruled out.

%Fe	%Mn	$\langle d \rangle_{XRD}$ (nm)	$\langle d \rangle_{HRTEM}$ (nm)	$\langle d \rangle_{TEM}$ (nm)	$\langle d \rangle_{HYD}$ (nm)	H_C (Oe)	M_R (emu· g^{-1})	M_{SAT} (emu· g^{-1})	T_B (K)	T_{SEP} (K)
*89% +88%	*11% +12%	14	15	50	54	29 (@310K) 80 (@5K)	6.4 (@310K) 13.5 (@5K)	32.7 (@310K) 42.4 (@5K)	372	>400

Table S1. Main compositional, structural, and magnetic parameters for the Mn-doped iron oxide CNCs. The degree of Mn doping in the clusters was assessed both by ICP (*) and EDS (+) analysis. The aver-age size of the primary nanocrystals was determined by XRD and HREM, whereas the average size of the secondary structures was assessed by TEM and DLS. The main magnetic parameters (coercive field, H_C; residual magnetization M_R; saturation magnetization M_{SAT}) were determined from hysteresis cycles at 5K and 310 K, whereas the blocking temperature (T_B) was inferred by ZFC-FC magnetization curves. It should be noted here that the Mn-doped iron oxide clusters were measured by ICP one year after their preparation and similar values for Fe and Mn were obtained (Fe: 87.2% and Mn 12.8%) indicating that Mn does not leak out of the clusters.

S3. ^{1}H Relaxivity values of Mn-doped iron oxide clusters: dependence from the magnetic field.

Sample	20 MHz			40 MHz			60 MHz		
	Relaxivity ($mM^{-1}s^{-1}$)		r_2/r_1	Relaxivity ($mM^{-1}s^{-1}$)		r_2/r_1	Relaxivity ($mM^{-1}s^{-1}$)		r_2/r_1
	r_1	r_2		r_1	r_2		r_1	r_2	
Mn-Doped CNC	27.5	571	20.7	13.6	536	39.4	7.7	503	65.3

Table S2. Longitudinal and Transverse ^{1}H Relaxivities (r_1, r_2) and r_2/r_1 of Mn-doped CNC under different frequency.

S4. SAR values of Mn-doped iron oxide cluster: dependence from magnetic field.

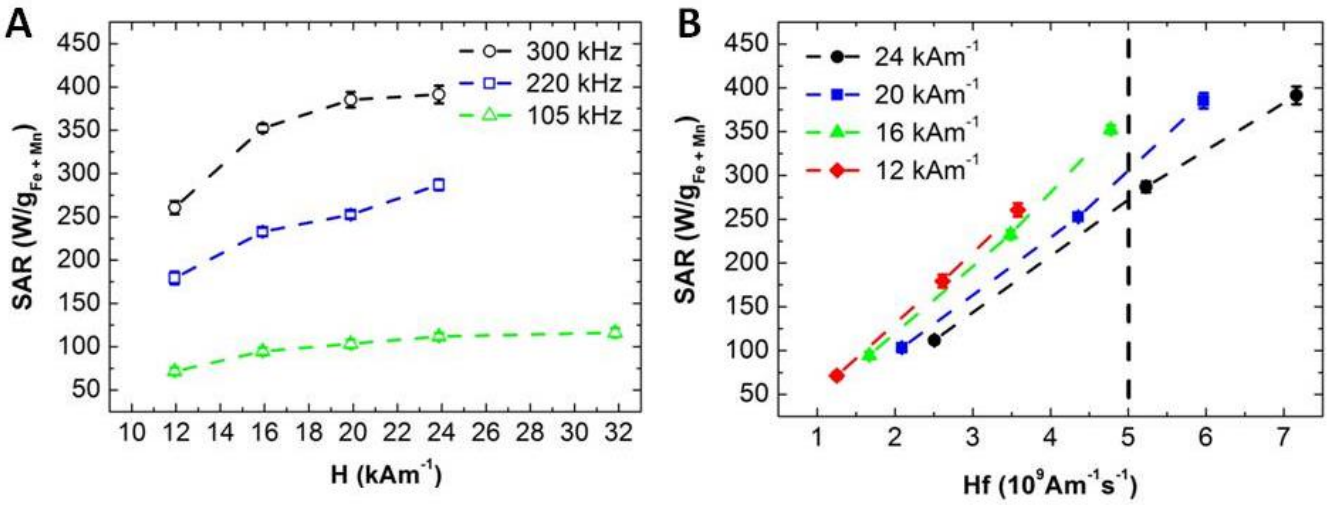

Figure S4. SAR values as a function of the magnetic field amplitude at three different frequencies (105-220 and 300 kHz) for Mn-doped CNCs with hydrodynamic size of 45 nm (A). SAR values as a function of the factor Hf at four different magnetic field amplitudes (12-16-20 and 24 kA m^{-1}) for the same doped-CNCs (B). The error bars indicate the standard deviation (in some case they are so small that they are not visible). The vertical black dashed line defines the biological limit (Hf = 5 x 10^9 A m^{-1} s^{-1}).

S5. SAR values of Mn-doped iron oxide cluster from temperature kinetic curves.

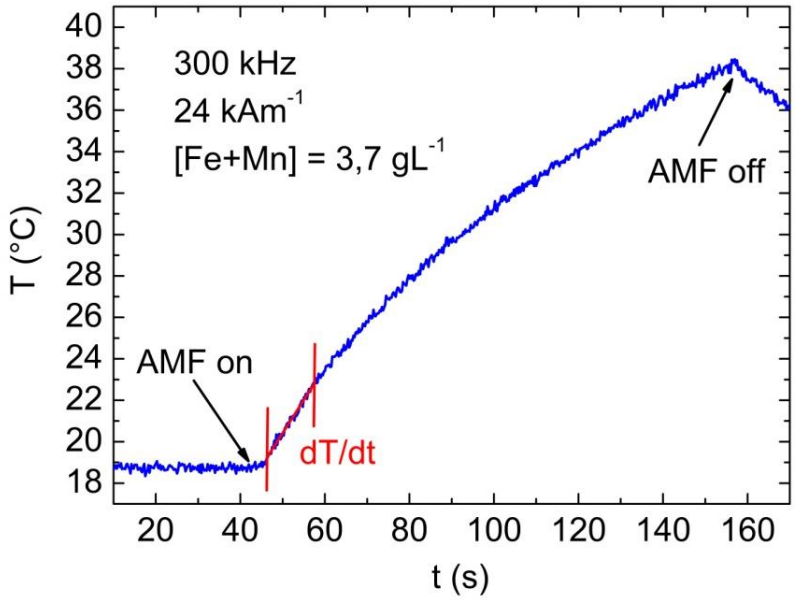

Figure S5. A typical temperature (T) versus time (t) curve of an aqueous dispersion of Mn-doped nanoclusters with a concentration set at Fe + Mn of 3.7 g/L is reported. The curve is recorded at 300 kHz and 24 kAm^{-1}. Since the measurement is performed in non-strictly adiabatic conditions, to minimize heat loss the slope dT/dt for the SAR calculation is determined taking into account only the linear part of the curve delimited by the two red lines (within the first seconds).

S6. SAR values and physico-chemical characterization of undoped iron oxide clusters.

Iron oxide clusters were prepared following a protocol similar to the synthesis of Mn-doped clusters. In particular, 50 mmol of anhydrous NaOH were reacted under N_2 flow with 20 mL of diethylene glycol at 120 °C for 1 hour while refluxing under vigorous stirring, and then cooled to 70 °C. 3.4 mL of the NaOH /DEG solution were then injected to a solution obtained by dissolving 0.8 mmol of anhydrous $FeCl_3$ and 8 mmol of polyacrylic acid in 34 mL DEG. The mixture was heated to 220 °C. After 1 hour the reaction was quenched and the iron oxide CNCs were collected after three cycles of purification and redispersion in water.

The obtained iron oxide particles show the expected arrangement into flower-like clusters, as shown in Figure S7, and statistical analysis of TEM images provides an average cluster size of 68±10 nm. The XRD pattern (see Fig S7) exhibits the typical spinel pattern for Fe_3O_4, and the average crystallite size as determined by line broadening yields a value of 10 ±1 nm. Morphological characterization indicates that the pure Fe_3O_4 CNCs have relevant morphology to the Mn-doped CNCs. However the pure Fe_3O_4 CNCs are composed of smaller individual nanocrystals (~10 nm) and they are assembled in secondary structures with larger cluster size (~68 nm) than Mn-doped iron oxide nanoparticles.

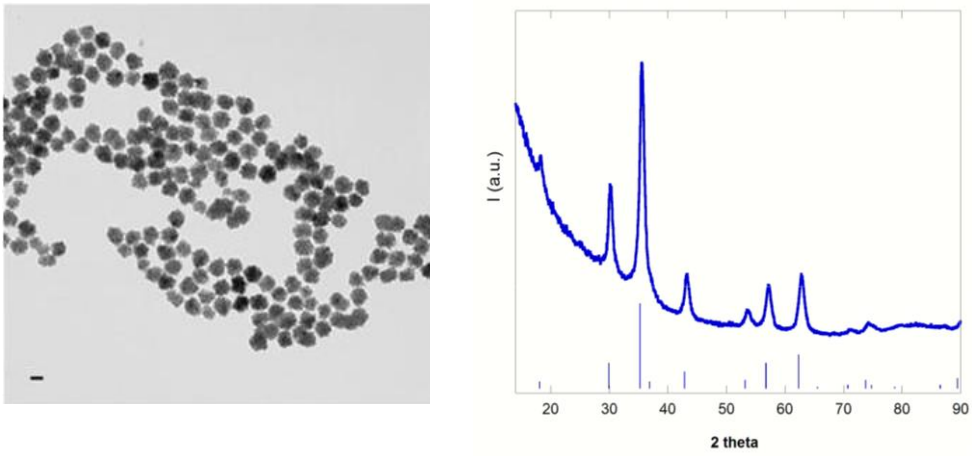

Figure S7. Representative TEM (left) and XRD pattern (right) of iron oxide CNCs. Scale bar in the TEM image is 50 nm. The experimental XRD pattern is compared to the reference PDF card #19-629 for pure bulk Fe_3O_4.

SAR measurements at different fields and frequencies were performed to assess the hyperthermic efficiency of the undoped Fe_3O_4 CNCs, as summarized in Table S3. The CNCs exhibit relevant SAR values, which as expected increase with the field intensity. The SAR values of undoped Fe_3O_4 CNCs are significantly (by a factor of ~3) smaller than those obtained for Mn-doped CNCs at all the experimental conditions.

F.(KHz)	*300*				*220*				*105*				
FIELD ($K \cdot Am^{-1}$)	*24*	*20*	*16*	*12*	*24*	*20*	*16*	*12*	*32*	*24*	*20*	*16*	*12*
SAR ($W \cdot g^{-1}$) *Fe_3O_4*	*149*	*133*	*109*	*100*	*90*	*84*	*74*	*69*	*50*	*45*	*40*	*26*	*21*

Table S3. Hyperthermic efficiency of the undoped Fe_3O_4 CNC as assessed by SAR determination under different field frequency and field amplitude.